

Anomalous collisional absorption of laser light in plasma using particle-in-cell simulations

M. Kundu

Institute for Plasma Research, Bhat, Gandhinagar - 382 428, Gujarat, India

(Dated: December 7, 2021)

Collisional absorption of laser light in a homogeneous, under-dense plasma is studied by a new particle-in-cell (PIC) simulation code considering one-dimensional slab-plasma geometry. Coulomb collisions between charge particles in plasma are modeled by a Monte Carlo scheme. For a given target thickness of a few times the wavelength of 800 nm laser of intensity I_0 , fractional absorption (α) of light due to Coulomb collisions (mainly between electrons and ions) is calculated at different electron temperature T_e by introducing a total velocity $v = \sqrt{v_{th}^2 + v_0^2}$ dependent Coulomb logarithm $\ln \Lambda(v)$, where v_{th} and v_0 are thermal and ponderomotive velocity of an electron. It is found that, in the low temperature regime ($T_e \lesssim 15$ eV), fractional absorption of light anomalously increases with increasing I_0 up to a maximum corresponding to an intensity I_c , and then it drops when $I_0 > I_c$. Such an anomalous variation of α with I_0 in the low intensity regime was demonstrated earlier in experiments, and recently explained by classical and quantum models [Phys. Plasmas **21**, 013302 (2014); Phys. Rev. E **91**, 043102 (2015)]. Here, for the first time, we report anomalous collisional laser absorption by PIC simulations, thus bridging the gap between models, simulations, and experimental findings.

PACS numbers: 52.50.Jm

I. INTRODUCTION

One of the main objectives of the researchers working in the field of laser-plasma interaction (LPI) is to couple more laser energy with the plasma (or matter) so as to obtain more energetic end-products, e.g., energetic charge particles or intense radiations. Therefore, it is of prime importance to know the underlying physical process (collisional and collisionless) by which laser energy is coupled to the plasma during the interaction. Earlier experiments [1–4] and theoretical studies [5–10] have already reported various absorption processes, e.g., linear resonance [11], anharmonic resonance [4, 12–18], Brunel heating [19, 20], skin layer absorption [21], $\mathbf{J} \times \mathbf{B}$ heating [22] etc., which often depend on parameters of the laser, and the plasma [7–10]. For example, while passing through under-dense plasma (where plasma frequency ω_p is less than the laser frequency ω) an intense p -polarized short laser pulse can be absorbed by exciting wake-fields and instabilities [7–10]. On the other hand, in an overdense plasma with an under-dense pedestal, linear resonance absorption (LR) of p -polarized light may occur by meeting the resonance condition $\omega_p = \omega$ in a specific location of the density gradient. Most often p -polarized light is used by experimentalists because of its ability to drive the plasma particles more efficiently, and relatively less attention is paid in LPI using s -polarized light. However, absorption of both s - and p -polarized light in plasma may happen through the electron-ion collision [7, 8, 23, 24] known as inverse bremsstrahlung (IB) if laser intensity is below 10^{17} Wcm $^{-2}$.

In this work, we concentrate on the absorption of a s -polarized laser light in a homogeneous, under-dense plasma-slab due to IB, since collisional and collisionless absorption processes are coupled together for a p -polarized light where it is difficult to know what fraction of the collisional absorption contributes to the total absorption. We are also motivated by some earlier experimental results [8, 25] of collisional absorption with s -polarized light which shows that fractional absorption α of light (i.e., ratio of absorbed energy to the in-

cident laser energy) anomalously increases initially with increasing laser intensity I_0 up to a maximum value about an intensity I_c , and then it drops nearly obeying the conventional scaling [7, 8], i.e., $\alpha \propto I_0^{-3/2}$. Although there are numerous analytical models [23–45] which directly or indirectly describe conventional (standard) collisional absorption (CA) without the effect of background plasma, less attempts were made to examine above mentioned anomalous collisional absorption (ACA). Recently, ACA process has been explained in the low temperature regime ($T_e \lesssim 15$ eV) by postulating a total velocity dependent Coulomb logarithm $\ln \Lambda(v)$ (where $v = \sqrt{v_{th}^2 + v_0^2}$, v_{th} and v_0 are the thermal and ponderomotive velocity) in an analytical model of electron-ion collision frequency ν_{ei} [35, 46] and more rigorous kinetic treatment [47]. However, to what extent this analytical approach is valid can only be answered numerically with self-consistent dynamics of plasma background under the laser irradiation. To this end, we have developed an one-dimensional electromagnetic particle-in-cell code (henceforth we call it EMPIC1D) where variation of physical quantities (charge density, current density, electro-magnetic fields) depend only on the one spatial coordinate along the laser propagation direction while considering all three velocity components of charge particles. In a particle-in-cell (PIC) simulation a reduced number of computational particles is used to represent plasma, instead of a large number of actual physical particles [48, 49]. This technique reduces the computational load, and enables to study the dynamics of an actual physical system of large number of charge particles. Sizes of these PIC particles (computational particles) are typically on the order of a numerical grid, they can pass through each other during the interaction, and Coulomb collisions do not naturally happen [50–56]. For this reason, Coulomb collisions are explicitly added in all PIC codes. To include Coulomb collision in our EMPIC1D code a Monte Carlo (MC) technique proposed by Takizuka and Abe [52] is adopted. Recently, this scheme is used in the PARASOL electrostatic PIC code [53] to study kinetic effects in tokamak

plasmas. It conserves total energy and total linear momentum before and after a collision event in the velocity space.

In this work, with the Monte Carlo collision assisted EMPIC1D code, for the first time we show the aforementioned anomalous absorption in an under-dense plasma in the low temperature regime similar to our earlier analytical works [46, 47]. Thus we bridge the gap between the experimental findings, analytical models, and PIC simulations.

Plasma is assumed to be pre-ionized. Laser intensity is kept below 10^{18} Wcm^{-2} so that relativistic effects are less important. For convenience, atomic units (a.u.) are used unless mentioned explicitly, i.e., $-e = m = 4\pi\epsilon_0 = \hbar = 1$, where $|e|$ is the electronic charge and mass, ϵ_0 is the permittivity of free space, and \hbar is the reduced Planck constant.

This article is organized in the following manner. Details of the EMPIC1D code is given in Sec.II, with appropriate benchmarking in the absence of collision. In Sec.III we independently benchmark the Monte Carlo (MC) binary collision scheme. Then we combine the collision module with the EMPIC1D code, and study collisional absorption of a s -polarized light in an under-dense plasma slab in Sec.IV where a comparison is also made between simulation and theoretical results. A summary is given in Sec.V.

II. DETAILS OF THE PIC CODE

Here we give only necessary details of the PIC code. In PIC a collection of physical particles is represented by a computational particle so that the charge to mass ratio q/m of the computational particle remains same as that of a physical particle. The following Maxwell-Lorentz system of equations (in the normalized form) is solved numerically after the discretization in space and time :

$$\frac{\partial \bar{\mathbf{B}}}{\partial t} = -c \nabla \times \mathbf{E}, \quad (1)$$

$$\frac{\partial \mathbf{E}}{\partial t} = c \nabla \times \bar{\mathbf{B}} - 4\pi \mathbf{J}, \quad (2)$$

$$\dot{\mathbf{p}} = q \left(\mathbf{E}_p + \mathbf{v} \times \frac{\bar{\mathbf{B}}_p}{c} \right). \quad (3)$$

Here, $\mathbf{E}, \bar{\mathbf{B}}$ are the electric and magnetic part of the electromagnetic field, \mathbf{p} is the particle momentum corresponding to its velocity \mathbf{v} and position \mathbf{r} at a time t . \mathbf{J} is the current density vector, c is the speed of light in the free space. The scaling $\bar{\mathbf{B}} = c\mathbf{B}$ connects actual magnetic field \mathbf{B} with the scaled magnetic field $\bar{\mathbf{B}}$. The other equations, namely, $\nabla \cdot \bar{\mathbf{B}} = 0$ and the Gauss's law $\nabla \cdot \mathbf{E} = 4\pi\rho$ are not explicitly solved in a standard multi-dimensional PIC scheme, thus saving a substantial amount of computer time. However, $\nabla \cdot \bar{\mathbf{B}} = 0$ is ensured by choosing a staggered grid, called Yee mesh. The charge and current conservation follows from $\partial\rho/\partial t + \nabla \cdot \mathbf{J} = 0$, thus ensuring $\nabla \cdot \mathbf{E} = 4\pi\rho$. Note that $\mathbf{E}, \bar{\mathbf{B}}, \mathbf{J}, \rho$ are calculated on the grid points. Therefore $\mathbf{E}, \bar{\mathbf{B}}$ field are interpolated to obtain corresponding fields $\mathbf{E}_p, \bar{\mathbf{B}}_p$ at the particle (particle charge q and mass m) position \mathbf{r} using linear weighting scheme, and the Lorentz equation (3) is solved using the standard leap-frog

method. The advantage of the scaling $\bar{\mathbf{B}} = c\mathbf{B}$ is that, it reduces equations (1) and (2) identical in form in the free space (i.e., when $\mathbf{J} = 0$) and the amplitudes of $\mathbf{E}, \bar{\mathbf{B}}$ becomes comparable. From now onward, for convenience, we shall write \mathbf{B} in stead of $\bar{\mathbf{B}}$ unless mentioned explicitly. A typical cycle of the PIC simulation is shown in Fig.1 which clearly depicts where the binary collision module (the MC part) should be incorporated.

A. Simplification in one-dimension

Let us consider a s -polarized light (propagating in y -direction) with transverse field components E_z, B_x . The physical quantities (e.g., charge density, current density, electromagnetic fields) are assumed to depend only on the space co-ordinate y , while retaining all three velocity components (v_x, v_y, v_z) of particles. Components of Eqn.(1)-(2) reads

$$\frac{\partial B_x}{\partial t} = -c \frac{\partial E_z}{\partial y}, \quad (4)$$

$$\frac{\partial E_z}{\partial t} = -c \frac{\partial B_x}{\partial y} - 4\pi J_z(t, y), \quad (5)$$

$$\frac{\partial E_y}{\partial t} = -4\pi J_y(t, y). \quad (6)$$

Equation (6) gives longitudinal component of the electric field E_y in our case. It is important to mention that, the numerical implementation of our PIC code is little different from some of the traditional 1D-PIC codes, namely, EM1BND [48], LPIC++ [10, 57], but closely follow the implementation in PIC codes PSC [58], VLPL [59], VPIC [60], OSIRIS [61], and VORPAL [62]. In EM1BND [48] and LPIC++ [10, 57], by performing addition and subtraction of Eqn.(4) and (5), and writing $\psi_{\pm} = E_z \pm B_x$ one finds $(\partial_t \pm c\partial_y)\psi_{\pm} = -4\pi J_z(t, y)$; where ψ_{\pm} can be recognized as the two propagating solutions of the wave equation. The advantage in this traditional procedure [10, 48, 57] is that the partial derivative $(\partial_t \pm c\partial_y)$ can be written in terms of the total derivative in time w.r.t. an observer moving at a speed $\pm c$, leading to

$$\frac{d\psi_{\pm}}{dt} = -4\pi J_z(t, y). \quad (7)$$

For a given J_z , Eq.(7) is solved as an ordinary differential equation (ODE) to obtain transverse fields $E_z = (\psi_+ + \psi_-)/2$, $B_x = (\psi_+ - \psi_-)/2$ on the grid. It also allows larger time step $\Delta t = \Delta y/c$. The disadvantage is that, the longitudinal component E_y is obtained by solving the Poisson's equation $\partial E_y/\partial y = 4\pi\rho$ explicitly (not from Eq.(6)), and it needs a separate algorithm than solving the transverse components. Moreover, this traditional scheme is hard to extend in multi-dimensional case. In our EMPIC1D code we use FDTD (finite difference in time domain) method for the solution of all field components (both traverse and longitudinal), in stead of the traditional addition-subtraction method mentioned above. Thus we use only one kind of algorithm for E_z, B_x, E_y which is extendable to PIC simulations in higher dimensions as in Refs.[58–62]. Using FDTD procedure on the Yee mesh, and assuming $t = n\Delta t$, $y = k\Delta y$, Eqn.(4),(5),(6) can be written as

$$\frac{B_x^{n+1}(k+1/2) - B_x^n(k+1/2)}{\Delta t} = -c \frac{E_z^{n+1/2}(k+1) - E_z^{n+1/2}(k)}{\Delta y}, \quad (8)$$

$$\frac{E_z^{n+1/2}(k+1) - E_z^{n-1/2}(k+1)}{\Delta t} = -c \frac{B_x^{n+1}(k+1/2) - B_x^{n+1}(k-1/2)}{\Delta y} - 4\pi J_z^{n+1/2}(k+1), \quad (9)$$

$$\frac{E_y^{n+1/2}(k+1) - E_y^{n-1/2}(k+1)}{\Delta t} = -4\pi J_y^{n+1/2}(k+1). \quad (10)$$

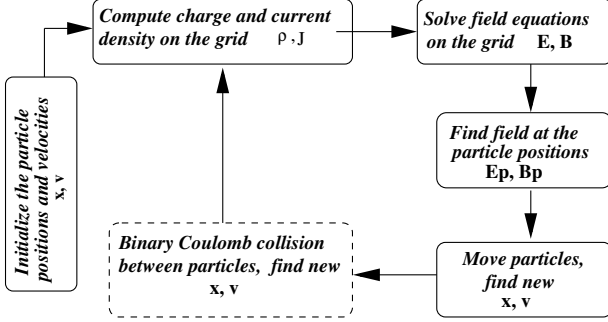


Figure 1. Schematic of a PIC simulation with binary collision.

To ensure numerical stability we take $c\Delta t/\Delta y = 1/2$, which decides the time step Δt for a chosen grid size Δy . The dispersion due to the FDTD discretization is minimized by choosing sufficient number of spatial grids (minimum 40 is taken) per wavelength of light. VLPL like [59] improvement, namely, dispersion free scheme we plan to include in future. The current density \mathbf{J} due to the motion of charge particles is computed using the “explicit current conserving scheme” by Umeda et al. [63] which satisfies $\partial\rho/\partial t + \nabla \cdot \mathbf{J} = 0$. Thus we avoid explicit solution of the Poisson’s equation to obtain E_y . We use “perfectly matched layer” (PML) absorbing boundary condition [64] for the electromagnetic fields. For charge particles, however, depending upon physical situations, absorbing, periodic, and reflecting boundary conditions are used.

B. Benchmarking of the PIC code

The EMPIC1D code is verified for different cases (where analytical solutions exist) : (i) plasma oscillation and energy conservation (without external light source), (ii) reflection of the laser light interacting with an over-dense plasma and corresponding field in the skin layer, (iii) transmission and reflection coefficient of laser light in an under-dense plasma, and (iv) interaction of light with inhomogeneous plasma and formation of standing waves. As a representative case, for the purpose of benchmarking, here we consider only the last case.

1. Interaction of *s*-polarized light with inhomogeneous plasma

Consider the interaction of a laser light with an inhomogeneous plasma which consists of an under-dense region and

an over-dense region separated by a critical density ($\rho_c = \omega^2/4\pi$) surface, illustrated in Fig.2. This problem was investigated analytically in Refs.[7, 8, 65] for time independent case. However its numerical verification with PIC method is still rare in the literature. Benchmarking of this problem *alone* can justify the correctness of interaction of laser field with under-dense and over-dense plasma in a single simulation run using EMPIC1D. We assume that density variation of plasma is linear $\rho_0(y) = \rho_c y/L$ along the propagation direction y of a *s*-polarized light described by E_z, B_x . L is the distance of the critical density surface (vertical dashed line) from the vacuum plasma interface on the left side. A continuous laser light $E_0 \sin(\omega t)$ of amplitude E_0 is sourced through the vacuum plasma interface. After propagating through the under-dense region $\rho_0(y)/\rho_c < 1$, light is reflected from the critical surface. The reflected light and the incident light are superimposed to form a standing wave after a long time when steady state is reached, and the resultant field E_z satisfies the wave equation [7, 8] $\frac{d^2 E_z}{d\eta^2} - \eta E_z = 0$ with $\eta(y) = (\omega^2/c^2 L)^{1/3}(y - L)$. Analytical solution $E_z(\eta) = c_1 \text{Ai}(\eta) + c_2 \text{Bi}(\eta)$ is found in terms of Airy functions Ai, Bi with c_1, c_2 as constants (independent of η). For the standing wave solution $c_2 = 0$ is chosen, since $\text{Bi} \rightarrow \infty$ as $\eta \rightarrow \infty$, leading to $E_z(\eta) = c_1 \text{Ai}(\eta)$. In reality, the problem is time dependent. Desired steady state analytical solution may not be reached during the early time of interaction. The constant c_1 depends upon the amplitude and phase of the resultant wave at the vacuum plasma interface at a given instant of time. We adjust c_1 with the effective magnitude of the field $E_s^{t_n}$ at a time $t = t_n$ retrieved from the PIC simulation at the vacuum plasma interface (at y_l) to match the analytical solution with the PIC simulation such that $c_1(t_n) = E_s^{t_n}(y_l)/\text{Ai}(\eta(y_l))$. It leads to the analytical solution as $E_z^{t_n}(y) = [E_s^{t_n}(y_l)/\text{Ai}(\eta(y_l))] \text{Ai}(\eta(y))$.

We take laser field parameters as $E_0 = 0.2$ a.u. , and $\omega = 0.057$ a.u. corresponding to $I_0 \approx 7 \times 10^{15} \text{ Wcm}^{-2}$ and $\lambda = 800$ nm respectively. The length of the simulation box is $L_b = 1000\Delta$ ($\Delta = \Delta y = \lambda/40$ is the grid size) with total number of grids $N_g = 1000$. Out of these 1000 grids, plasma particles centrally occupy 990 grids while 5 grids are left on each boundaries to separate the plasma from the vacuum. The source is located at the left plasma vacuum interface at $y = y_l = 5\Delta$. The right boundary of the plasma is at $y = y_r = 995\Delta$. There are $N = 7920$ PIC ions (assumed to be stationary) each of charge $q_s = 0.00325$ a.u. and an equal number of overlapping PIC electrons with mass $m_s = q_s$, and charge $-q_s$. Particles are loaded according to the scheme given in Ref.[48] to obtain a linear density profile as shown

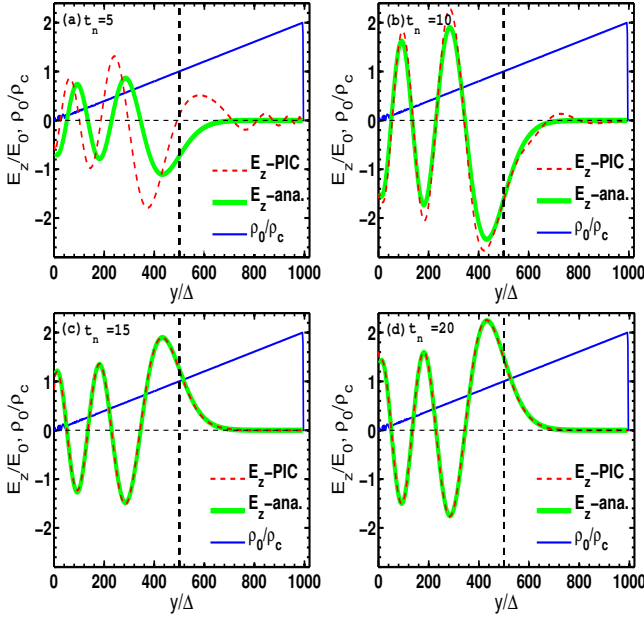


Figure 2. (Color online) Formation of standing wave solution due to the interaction of s-polarized light with inhomogeneous plasma of linear density profile ρ_0/ρ_c (dark solid line, blue). Vertical dashed line is the critical density layer. At an early time $t_n = 5$ in (a) the profile of the laser field E_z in the PIC simulation (dashed oscillatory line, red) is far from the steady state Airy profile (solid gray line, green). As time increases difference between PIC profile and the analytical profile gradually decreases which is clear from (a) and (b). After a long time, e.g., $t_n = 15, 20$ in (c,d) PIC result matches the desired analytical Airy profile.

in Figs.2(a)-(d) with ρ_0/ρ_c rising linearly from 0 to 2 (dark solid line, blue). The field profiles E_z/E_0 from PIC simulation (dashed oscillatory, red) and the analytical solution (solid oscillatory, green) are plotted against y/Δ in Figs.2(a-d) at different times $t_n = 5, 10, 15, 20$ respectively. At an early time $t_n = 5$, PIC solution for E_z does not match with the analytical solution (in Fig.2a) since at this early time superposition of the reflected wave with the incident wave is still incomplete in the PIC simulation to form the desired standing wave. As time increases, difference between the PIC profile and the analytical profile gradually decreases which is evident from the comparison between Fig.2a and Fig.2b. After a sufficiently longer time $t_n = 15$ and beyond, the reflected wave meets the incident wave with required amplitude and phase so that the PIC solution matches (in Figs.2c,d) the analytical solution (see oscillatory dashed line coincides the solid line). The match between analytical and the numerical solution clearly ensures the correctness of our PIC simulation without collision.

III. BINARY COLLISION: MODEL AND SIMULATION

In the PIC simulation, as discussed above, particles may pass through each other during their close encounter and collision effects are omitted. To implement binary collision in the EMPIC1D code we have followed the Monte Carlo scheme

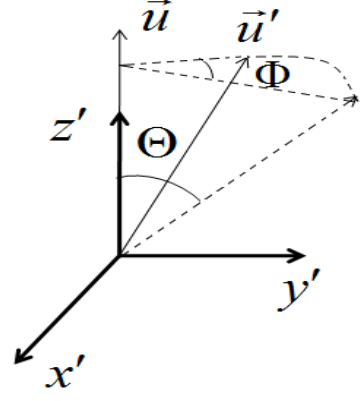


Figure 3. Relative velocities (\vec{u}, \vec{u}') before and after the collision.

given by Takizuka and Abe [52] and also the work by Ma et al. [54], and Sentoku et al. [50]. For conciseness we only show the validation of our implementation with a minimum detail. The main approximation of binary collision is that at a given instant only two particles will collide, and the effect of collision arises due to the cumulative effect of many small angle binary collisions. Within a computational cell, particles are paired randomly (ion-ion, ion-electron, electron-electron) and then collision is performed between every pair. The maximum impact parameter in a fully ionized quasi-neutral plasma being of the order of the Debye length [66], the maximum size of the collision grid is also restricted to the Debye length. Collision event takes place in the velocity space, meaning that the velocity components of the particles changes but the coordinates are not influenced at that time. The post collision velocities are obtained by going to the center of mass (COM) frame of the respective collision pairs and then back to the laboratory frame. Due to collision, during a small time interval Δt_c (which is sufficiently small compared to the mean relaxation time), the direction of velocities of the colliding particles changes but not their magnitudes. For instance, we consider a system of two particles from two species α and β having velocities v_α and v_β , masses m_α and m_β , densities n_α and n_β , and charges e_α and e_β . At a given instant t , the effect of collision leads to the rotation of the relative velocity $\mathbf{u} = \mathbf{v}_\alpha - \mathbf{v}_\beta$ in the COM frame of the two particles. The relative velocity $\mathbf{u}' = \mathbf{v}'_\alpha - \mathbf{v}'_\beta$ after the collision (primes represents quantities after collisions) in the COM frame, and the rotation of the velocity vector $\mathbf{u} \rightarrow \mathbf{u}'$ can be described by the scattering angle Θ and the azimuth angle Φ (see Fig.3) which are chosen randomly for a given pair (α, β) . In order to find Θ , a parameter δ is introduced such that $\delta = \tan(\Theta/2)$. The variable δ is chosen randomly from a Gaussian distribution such that its mean is zero, and corresponding variance $\langle \delta^2 \rangle$ is [52–54]

$$\langle \delta^2 \rangle = \frac{e_\alpha^2 e_\beta^2 n_L \ln \Lambda}{8\pi \epsilon_0^2 m_\alpha^2 m_\beta^2 u^3} \Delta t_c. \quad (11)$$

Here n_L is the minimum density between n_α and n_β , $m_{\alpha\beta} = m_\alpha m_\beta / (m_\alpha + m_\beta)$ is the reduced mass, and $\ln \Lambda$ is the

Coulomb logarithm. $\ln \Lambda$ can be calculated as [66]

$$\ln \Lambda = \ln[\lambda_D(T_\alpha + T_\beta)/2e_\alpha e_\beta] \quad (12)$$

where λ_D is the Debye length, and T_α, T_β are the temperatures of the respective species. Above expression of $\ln \Lambda$ is valid in the absence of external laser field. Otherwise, $\ln \Lambda$ should include the response of electrons to the laser field strength E_0 and the frequency ω . We shall use Eq.(12) only for the validation of binary collision event when there is no external force. The necessary modification of $\ln \Lambda$ with laser field will be discussed later. Deflection angle Θ is calculated by using Box-Muller method with distribution $p(\delta)d\delta = (1/\langle\delta^2\rangle)\exp(-\delta^2/2\langle\delta^2\rangle)\delta d\delta$ as given in Refs.[67, 68],

$$\Theta = 2 \arctan \sqrt{-2\langle\delta^2\rangle \ln(1-R_1)}, \quad (13)$$

where R_1 is a uniform random number between 0 and 1. The azimuth angle Φ is chosen as $\Phi = 2\pi R_2$, with R_2 as a uniform random number between 0 and 1. The change in velocity components in the laboratory frame can be calculated as [52]

$$\begin{aligned} \Delta u_x &= \frac{u_x}{u_\perp} u_z \sin \Theta \cos \Phi - \frac{u_y}{u_\perp} u \sin \Theta \sin \Phi \\ &\quad - u_x(1 - \cos \Theta) \end{aligned} \quad (14)$$

$$\begin{aligned} \Delta u_y &= \frac{u_y}{u_\perp} u_z \sin \Theta \cos \Phi + \frac{u_x}{u_\perp} u \sin \Theta \sin \Phi \\ &\quad - u_y(1 - \cos \Theta) \end{aligned} \quad (15)$$

$$\Delta u_z = -u_\perp \sin \Theta \cos \Phi - u_z(1 - \cos \Theta) \quad (16)$$

where $u_\perp = \sqrt{u_x^2 + u_y^2}$. When $u_\perp = 0$, we take

$$\Delta u_x = u \sin \Theta \cos \Phi, \quad (17)$$

$$\Delta u_y = u \sin \Theta \sin \Phi, \quad (18)$$

$$\Delta u_z = -u(1 - \cos \Theta). \quad (19)$$

Final post collision velocities in the laboratory frame reads

$$\mathbf{v}_\alpha(t + \Delta t_c) = \mathbf{v}_\alpha(t) + (m_{\alpha\beta}/m_\alpha)\Delta \mathbf{u} \quad (20)$$

$$\mathbf{v}_\beta(t + \Delta t_c) = \mathbf{v}_\beta(t) - (m_{\alpha\beta}/m_\beta)\Delta \mathbf{u}. \quad (21)$$

A. Validation of the binary collision model

In order to validate our implementation of binary collision, we consider particle collisions in a two component plasma. The conservation of energy, and momentum for each colliding pair of particles are rigorously checked. We benchmark different relaxation rates (collision frequencies): (i) mean rate of change of velocity of the electrons (called slowing down frequency ν_s), (ii) mean rate of change of energy of the test electrons (energy transfer frequency, ν_t), and (iii) the rate of spread of the test particle velocity transverse to its original direction (deflection frequency, ν_d). Analytically, these frequencies are obtained by the test particle theory [66, 69] in which a test particle (electron, designated by α) is assumed to move through a medium of field particles (ions, designated by

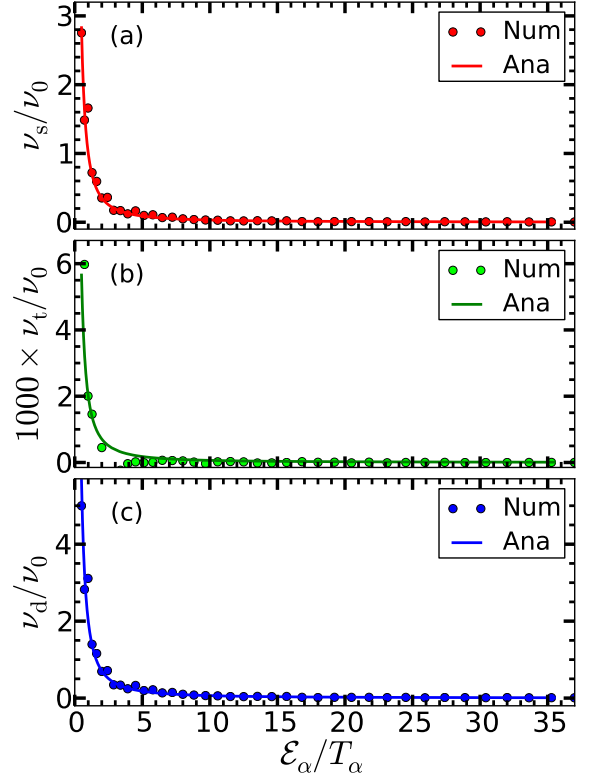


Figure 4. Normalized (a) slowing down frequency ν_s , (b) energy transfer frequency ν_t , and (c) deflection frequency ν_d vs normalized energy $\mathcal{E}_\alpha/T_\alpha$ of electrons due to Coulomb collision with background ions after $n_t = 20$ time steps. Each numerical point represents one group of particles (out of total 40 groups) each having 250 particles. Solid lines are analytical results using Eqns.(25)-(27) while circles represent respective numerical results.

β) having Maxwellian velocity distribution. These frequencies are related to the transport equations [66, 69]

$$\left\langle \frac{d\mathbf{v}_\alpha}{dt} \right\rangle = -\nu_s \mathbf{v}_\alpha, \quad (22)$$

$$\left\langle \frac{d\mathcal{E}_\alpha}{dt} \right\rangle = -\nu_t \mathcal{E}_\alpha, \quad (23)$$

$$\left\langle \frac{d\mathbf{v}_\perp^2}{dt} \right\rangle = \nu_d \nu_\alpha^2, \quad (24)$$

and can be expressed in terms of the integral $\mu(x) = \frac{2}{\pi} \int_0^x \sqrt{t} \exp(-t) dt$ and its derivative $\mu'(x) = \frac{2}{\pi} \sqrt{x} \exp(-x)$ as

$$\nu_s = \nu_0 (1 + m_\alpha/m_\beta) \mu(x) \quad (25)$$

$$\nu_t = 2\nu_0 (m_\alpha \mu(x)/m_\beta - \mu'(x)) \quad (26)$$

$$\nu_d = 2\nu_0 (\mu(x) + \mu'(x) - \mu(x)/2x). \quad (27)$$

Here $\nu_0 = e_\alpha^2 e_\beta^2 n_\beta \ln \Lambda / (8\pi \epsilon_0^2 \sqrt{2m_\alpha \mathcal{E}_\alpha^3})$ is the basic collision frequency, $\mathcal{E}_\alpha = m_\alpha v_\alpha^2/2$ is the kinetic energy of the projectile, and $x = m_\beta \mathcal{E}_\alpha / m_\alpha T_\beta$. To obtain ν_s, ν_t, ν_d an average over a group of test particles (electrons) having the same velocity are taken for the better statistics.

We consider 10000 test particles (electrons) and an equal number of field particles (ions). Test particles are assumed to be composed of 40 groups, and each of 250 particles in a group has the same initial velocity. Their velocities are normalized by the thermal velocity, $v_{th} = \sqrt{T_\alpha/m_\alpha}$. Here we assume $m_\beta/m_\alpha = 10000$ (i.e. the field particles are highly massive), $T_\alpha = T_\beta = T = 5$ eV, $e_\alpha = e_\beta = e$ (charge of the electron), $n_\alpha = n_\beta = n_d = 10^{15} \text{ cm}^{-3}$, and $v_0\Delta t_c = 10^{-3}$. The value of $v_0\Delta t_c$ is chosen small to ensure small angle collisions [54]. In the Monte Carlo simulation, v_s, v_t, v_d are calculated using the Eqn.(22),(23), and (24) with the velocities from Eqn.(20), and (21) before and after collisions.

Figure 4 shows the normalized frequencies ($v_s/v_0, v_t/v_0$, and v_d/v_0) versus the energy of the test particles $\mathcal{E}_\alpha/T_\alpha$ after $n_t = 20$ time steps. Each solid circle (numerical) represents the average over a group of test particles. An excellent agreement between the numerical results and the analytical values (solid lines) from Eqn.(25),(26), and (27) ensures the correctness of our implementation.

IV. ABSORPTION IN AN UNDER-DENSE PLASMA

We have integrated the above collision module with the EMPIC1D code described in Sec.II to study collisional absorption of light incident normally on an under-dense plasma slab of uniform density. The simulation domain consists of $N_g = 500$ computational cells with the plasma slab at the center. Initially each computational cell contains equal number of electrons and ions so that plasma is charge neutral. The temporal profile of the laser pulse (at the left boundary, y_l) is chosen as

$$E_z(t, y_l) = E_0 \begin{cases} \sin^2(\omega t/2n_c) \cos(\omega t); & 0 < t < n_c T \\ 0 & t > n_c T, \end{cases} \quad (28)$$

with n_c as the number of cycles, and $T = 2\pi/\omega$ as the laser period. The pulse is numerically excited at $y = y_l$, propagates in free space, then strikes the plasma slab. The intensity, wavelength, number of cycles, the duration of pulse, the width L_p of the plasma slab can be varied as desired. Accordingly the length of the computational domain, and the number of computational cells N_g are also adjusted. We choose the laser wavelength $\lambda = 800$ nm with $n_c = 4$ -cycles, and the total pulse duration ≈ 30 fs. The size of a computational cell is chosen as $\Delta = 200$ a.u. which yields the PIC time step $\Delta t_{PIC} = 0.729248$ a.u. Length of the plasma is chosen as $L_p \approx 1.32\lambda$ with a plasma density $\rho/\rho_c \approx 0.136$. Temperature of ions are kept fixed in all simulations at $T_i = 5$ eV while temperature of electrons are kept fixed at different values, e.g., $T_e = 5, 10, \dots, 50, 100$ eV for a given laser intensity. The chosen value of T_i , however, is found to have negligible effect on the overall results of collisional absorption. Above parameters are kept fixed during a simulation run unless mentioned explicitly. To simulate inverse bremsstrahlung absorption in presence of a laser field the Coulomb logarithm should not be same as Eq.(12) for ordinary collisions, since it does not include the laser field parameters. Because there is no unique

model of $\ln\Lambda$ in presence of laser field, we use a modified Coulomb logarithm [35, 40, 46]

$$\ln\Lambda = 0.5 \ln \left[1 + (b_{\max}/b_\perp)^2 \right], \quad (29)$$

where $b_{\max} = V_t/\max(\omega, \omega_p)$, $b_\perp = e^2/(4\pi\epsilon_0 m_e V_t^2)$, with $V_t^2 = v_{th,e}^2 + v_0^2$ as the total velocity. The effect of laser field is incorporated through the ponderomotive velocity $v_0 = eE_0/m_e\omega$. In the absence of laser field, $V_t = v_{th,e}$, $b_{\max} = V_t/\omega_p = \lambda_D$ and $\ln\Lambda$ in Eq.(29) becomes nearly equal to that given in Eq.(12).

From the simulation, we record total kinetic energy ke gained by the particles, the electric part $ee = \sum_1^{N_g} E_j^2 \Delta/8\pi$ and the magnetic part $me = \sum_1^{N_g} B_j^2 \Delta/8\pi$ of the electromagnetic energy at every time step, giving the total energy $te = ke + ee + me$. Figure 5 shows temporal variation of various energies at a given laser intensity $I_0 = 5 \times 10^{14} \text{ Wcm}^{-2}$ for the two cases: (a) without collision, and (b) with collision between electrons and ions. In Figs.5 (a)-(b) for the initial time upto $t/T \approx 3$, all energies ee, me , and te increase sharply since the laser pulse is entering the simulation domain. For $t/T \approx 3-4$ the value of ee, me remains almost constant and te reaches a maximum because entire pulse has appeared in the simulation domain. The pulse strikes the plasma slab about $t/T \approx 4$, and only after this time, for $t/T = 4-7.5$, ke first increases and then drops with the corresponding drop and increase in ee , and me while te remain conserved at the highest value. After $t/T \approx 7.5$, values of ee, me and te sharply drop since the laser pulse is leaving the finite simulation domain, and gets absorbed (artificially) in the right boundary. The constant value of total energy, when the entire pulse is inside the computational box (for $t/T = 3-7.5$), indicates conservation of energy in the simulation. In Fig.5(a), without collision, ke reaches a maximum value, and finally drops to zero before $t/T \approx 7.5$. This is expected, because particles can not retain this energy, and finally give back to the electromagnetic fields (which is also evident from the corresponding drop and rise of ee and me between $t/T = 4-7.5$), resulting no net absorption. However, when collision is taken into account [in Fig.5(b)] ke increases monotonically in time starting at $t/T \approx 4$ (with corresponding drop in ee and me , meaning absorption of the pulse), and reaches a non-zero saturation value around $t/T = 6.8$ much before the pulse has left the simulation box. ke does not drop to zero even after the pulse is over which clearly shows that s-polarized light can be absorbed due to collisions and the laser energy can be transferred to the charge particles.

We now find nature of collisional absorption by varying the intensity of the laser pulse for a given initial temperature T_e . In reality, T_e should also vary during the interaction. But our pulse being very short we assume it to be unchanged. The other parameters, such as plasma thickness L_p , plasma density ρ , ion temperature T_i are kept constant as above.

Figure 6 shows fractional absorption α , defined as the ratio of the final kinetic energy retained in the particles to the maximum of te (which is actually the total energy in the laser pulse), versus the peak intensity for $T_e = 5, 10, 50, 100$ eV (solid lines). It is seen that, for higher temperatures $T_e >$

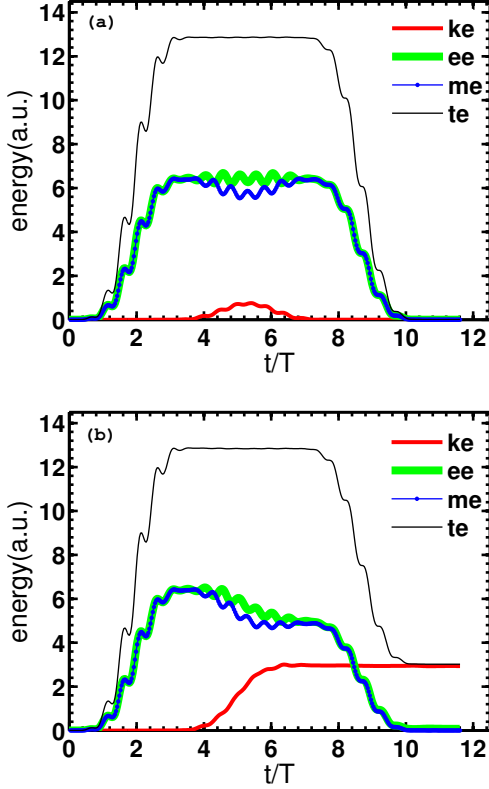


Figure 5. Different energy profiles (kinetic energy ke , electric part $ee = \sum E_j^2 \Delta / 8\pi$, magnetic part $me = \sum B_j^2 \Delta / 8\pi$ of the electromagnetic energy, and the total energy $te = ke + ee + me$) vs normalized time t/T for s -polarized light interacting with an under-dense plasma. Without collision energy is not absorbed (in a) finally. With collision (in b) laser energy is absorbed, and transferred to the particle kinetic energies (see $ke \neq 0$) in the end of the interaction.

20 eV, α initially remains almost constant (or vary slowly) upto a certain value $I_c \approx 6 \times 10^{13} \text{ Wcm}^{-2}$ of the peak intensity, and then decreases gradually for intensities $I_0 > I_c$. This is the conventional result of collisional absorption reported in earlier works [23, 24, 70] with a $\ln \Lambda$ independent of the ponderomotive velocity $v_0 = E_0/\omega$. However, at a lower $T_e < 20$ eV, it is found that α initially increases with the intensity, reaches a maximum value about an intensity I_c , then drops similar to the high temperature case. Such an anomalous behavior (initial increase followed by a drop) of fractional absorption versus the laser intensity was reported experimentally with normally incident s -polarized light (of wavelengths 800 nm [8] and 268 nm [25]) on an under-dense plasma with the peak absorption more than 30%. Incorporating a total velocity dependent $\ln \Lambda$, in our EMPIC1D code assisted by Monte Carlo binary collision we reproduce similar anomalous nature of collisional absorption in the low temperature regime. Our results indicate that fractional absorption due to collisional processes can be as high as 40% or even more for different plasma and laser parameters. For the shake of completeness, numerical results are compared with analytical estimates (dashed line in Fig.6) using a modified $\ln \Lambda$ as in Eq.(29) in the ballistic model

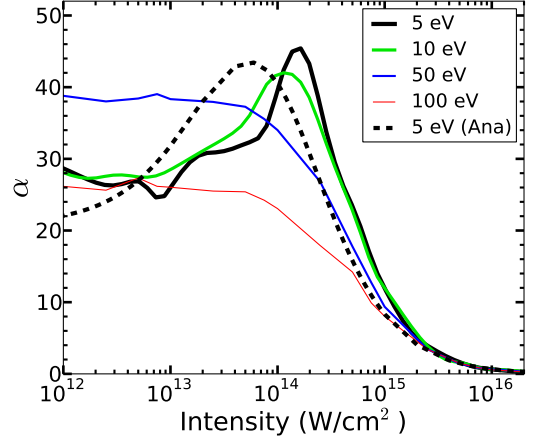


Figure 6. Fractional absorption vs peak laser intensity, for s -polarized light interacting with an the under-dense plasma as in Fig.5 at $T_e = 5, 10, 50, 100$ eV (numerical, solid line) and at $T_e = 5$ eV (analytical, dashed line, using Eq.(31)).

[35, 46] of time-dependent electron-ion collision frequency

$$v_{ei}(t) = \frac{\omega_p^2 \ln \Lambda}{v_{os}^3(t)} \left[\text{erf}(u(t)) - \frac{2}{\sqrt{\pi}} u(t) e^{-u(t)^2} \right]. \quad (30)$$

Where $u(t) = v_{os}(t)/\sqrt{2}v_{th}$, and $v_{os}(t)$ is oscillation velocity of the electron in the laser field. Averaging $v_{ei}(t)$ over a laser period leads to average \bar{v}_{ei} and fractional absorption

$$\alpha = 1 - \exp(-2\kappa_i L_p) \quad (31)$$

of a continuous light of frequency ω in an under-dense plasma slab [7, 8] at normal incidence. Here $\kappa_i = (\rho/\rho_c)\bar{v}_{ei}/v_g$, and $v_g = c\sqrt{1-\rho/\rho_c}$ is the group velocity of light. Analytical result using Eq.(31) (dashed line) at a lower temperature $T_e = 5$ eV shows qualitative agreement with the EMPIC1D result, and confirms the anomalous nature of collisional absorption which was also reported by quantum and classical kinetic models [46, 47]. However, there are discrepancies between numerical and analytical results at higher temperatures, which may be due to (i) time varying field experienced by particles, (ii) movement of ion back-ground to conserve momenta and energy during binary collisions in the numerical simulations as opposed to the analytical model where all particles experience same peak laser field E_0 , and ions are considered stationary.

V. SUMMARY

Collisional absorption of s -polarized laser light in a homogeneous, under-dense plasma is studied by a new particle-in-cell (PIC) simulation code considering one-dimensional slab-plasma geometry. To account for Coulomb collisions between charge particles a Monte Carlo (MC) binary collision scheme is used in the PIC code. For a given target thickness of a few times the wavelength of 800 nm laser fractional absorption of

light due to Coulomb collisions is calculated at different electron temperature T_e using a total velocity $v = \sqrt{v_{th}^2 + v_0^2}$ dependent Coulomb logarithm $\ln\Lambda(v)$. In the low temperature regime ($T_e \lesssim 15$ eV) it is found that fractional absorption (α) of light anomalously increases initially with increasing intensity I_0 up to a maximum value corresponding to an intensity I_c , and then it drops approximately obeying the conventional scenario, i.e., $\alpha \propto I_0^{-3/2}$ when $I_0 > I_c$. Anomalous increase of α with I_0 was demonstrated in some earlier experiments [8, 25], and recently explained by various models [46, 47] using total velocity dependent cut-offs. Here, we report anomalous nature of laser absorption by self-consistent PIC simulations

assisted by Monte-Carlo collisions, thus bridging the gap between the models, simulations, and experiments.

ACKNOWLEDGMENTS

The author would like to thank Anshuman Borthakur for the initial help in the Monte-Carlo simulations, the Plasma Science Society of India (PSSI) for providing partial financial support as a PSSI fellowship to carry out this work and Sudip Sengupta for valuable suggestions.

-
- [1] D. R. Bach, D. E. Casperson, D. W. Forslund, S. J. Gitomer, P. D. Goldstone, A. Hauer, J. F. Kephart, J. M. Kindel, R. Kristal, G. A. Kyrala, K. B. Mitchell, D. B. van Hulsteyn, and A. H. Williams, Phys. Rev. Lett. **50**, 2082 (1983).
 - [2] U. Teubner, J. Bergmann, B. van Wousterghem, F. P. Schäfer, and R. Sauerbrey, Phys. Rev. Lett. **70**, 794 (1993).
 - [3] D. F. Price, R. M. More, R. S. Walling, G. Guethlein, R. L. Shepherd, R. E. Stewart, and W. E. White, Phys. Rev. Lett. **75**, 252 (1995).
 - [4] M. Cerchez, R. Jung, J. Osterholz, T. Toncian, O. Willi, P. Mulser, and H. Ruhl, Phys. Rev. Lett. **100**, 245001 (2008).
 - [5] W. Rozmus and V. T. Tikhonchuk, Phys. Rev. A **46**, 7810 (1992).
 - [6] Q. L. Dong, J. Zhang, and H. Teng, Phys. Rev. E **64**, 026411 (2001).
 - [7] William L. Kruer, *The Physics of Laser Plasma Interactions*, (Addison-Wesley, New York, 1988).
 - [8] Shalom Eliezer, *The Interaction of High-Power Lasers with Plasmas*, (IOP Publishing, Bristol, 2002).
 - [9] Peter Mulser and Dieter Bauer, *High Power Laser-Matter Interaction*, STMP 238 (Springer, Berlin, Heidelberg 2010).
 - [10] Paul Gibbon, *Short Pulse Laser Interactions with Matter: An Introduction* (Imperial College Press, 2005).
 - [11] K. R. Manes, V. C. Rupert, J. M. Auerbach, P. Lee, and J. E. Swain, Phys. Rev. Lett. **39**, 281 (1977).
 - [12] P. Mulser, D. Bauer, and H. Ruhl, Phys. Rev. Lett. **101**, 225002 (2008).
 - [13] P. Mulser and M. Kanapathipillai, Phys. Rev. A **71**, 063201 (2005).
 - [14] P. Mulser, M. Kanapathipillai, and D. H. H. Hoffman, Phys. Rev. Lett. **95**, 103401 (2005).
 - [15] M. Kundu and D. Bauer, Phys. Rev. Lett. **96**, 123401 (2006).
 - [16] M. Kundu and D. Bauer, Phys. Rev. A **74**, 063202 (2006).
 - [17] M. Kundu, P. K. Kaw, and D. Bauer, Phys. Rev. A **85**, 23202 (2012).
 - [18] I. Kostyukov and J. M. Rax, Phys. Rev. E **67**, 066405 (2003).
 - [19] F. Brunel, Phys. Rev. Lett. **59**, 52 (1987).
 - [20] P. Mulser, S. M. Weng, and Tatyana Liseykina, Phys. Plasmas **19**, 043301 (2012).
 - [21] D. Bauer and P. Mulser, Phys. Plasmas **14**, 023301 (2007).
 - [22] Hong-bo Cai, Wei Yu, Shao-ping Zhu, and Chun-yang Zheng, Phys. Plasmas **13**, 113105 (2006).
 - [23] Th. Bornath, D. Kremp, P. Hilse, and M. Schlanges, Journal of Physics: Conference series **11**, 180 (2005).
 - [24] Th. Bornath, M. Schlanges, P. Hilse, and D. Kremp, Phys. Rev. E **64**, 26414 (2001).
 - [25] D. Riley, L. A. Gizzi, A. J. Mackinnon, S. M. Viana, and O. Willi, Phys. Rev. E **48**, 4855 (1993).
 - [26] L. Schlessinger and J. Wright, Phys. Rev. A **20**, 1934 (1979).
 - [27] P. Hilse, M. Schlanges, Th. Bornath, and D. Kremp, Phys. Rev. E **71**, 056408 (2005).
 - [28] J. T. Mendonça, R. M. O. Galvão, A. Serbeto, Shi-Jun Liang, and L. K. Ang, Phys. Rev. E **87**, 063112 (2013).
 - [29] M. Moll, M. Schlanges, Th. Bornath, and V. P. Krainov, New Journal of Physics **14**, 065010 (2012).
 - [30] G. J. Pert, J. Phys. A **5**, 506 (1972).
 - [31] G. J. Pert, J. Phys. B **8**, 3069 (1975).
 - [32] S. Rand, Phys. Rev. **136**, B231 (1964).
 - [33] Su-Ming Weng, Zheng-Ming Sheng, and Jie Zhang, Phys. Rev. E **80**, 56406 (2009).
 - [34] V. P. Silin, Sov. Phys. JETP **20**, 1510 (1965).
 - [35] P. Mulser and A. Saemann, Contrib. Plasma Phys. **37**, 211 (1997).
 - [36] P. Mulser and R. Schneider, J. Phys. A: Math. Theor. **42**, 214058 (2009).
 - [37] P. Mulser, F. Cornolti, E. Bésuelle, and R. Schneider, Phys. Rev. E **63**, 16406 (2000).
 - [38] H.-J. Kull and L. Plagne, Phys. Plasmas **8**, 5244 (2001).
 - [39] John Wesson, *Tokamaks*, (Oxford University Press, 2004).
 - [40] G. J. Pert, Phys. Rev. E **51**, 4778 (1995).
 - [41] S. C. Rae and K. Burnett, Phys. Rev. A **46**, 2077 (1992).
 - [42] P. J. Catto and Th. Speziale, Phys. Fluids **20**, 167 (1977).
 - [43] D. Kremp, Th. Bornath, P. Hilse, H. Haberland, M. Schlanges, and M. Bonitz, Contrib. Plasma Phys. **41**, 259 (2001).
 - [44] A. Brantov, W. Rozmus, R. Sydora, C. E. Capjack, V. Yu. Bychenkov et al., Phys. Plasmas **10**, 3385 (2003).
 - [45] S. Skupsky, Physical review A **36**, 5701 (1987).
 - [46] M. Kundu, Phys. Plasmas **21**, 13302 (2014).
 - [47] M. Kundu, Phys. Rev. E **91**, 043102 (2015).
 - [48] C. K. Birdsall and A. B. Langdon, *Plasma Physics via Computer Simulation*, (McGraw Hill, New York, 1981).
 - [49] R. W. Hockney and J. W. Eastwood, *Computer Simulation using Particles*, (IOP Publishing, Adam Hilger, New York, 1988).
 - [50] Y. Sentoku, K. Mima, Y. Kishimoto and M. Honda, Journal of Physical Society of Japan **67**, 4084 (1998); Y. Sentoku, A.J. Kemp, Journal of Computational Physics **227**, 6846 (2008).
 - [51] M. G. Cadjan and M. F. Ivanov, J. plasma phys. **61**, 89 (1999).
 - [52] T. Takizuka and H. Abe, J. Comput. Phys. **25**, 205 (1977).
 - [53] T. Takizuka, Plasma Phys. Control. Fusion **59**, 034008 (2017); T. Takizuka, K. Shimizu, N. Hayashi, M. Hosokawa, and M. Yagi, Nucl. Fusion **49**, 075038 (2009); T. Takizuka, Plasma Science and Technology **13**, 316 (2011).

- [54] S. Ma, R. D. Sydora and J. M. Dawson, *Comput. Phys. Commun.* **77**, 190 (1993).
- [55] W. M. Manheimer, M. Lampe and G. Joyce, *J. Comput. Phys.* **138**, 563 (1997).
- [56] T. A. Oliphant and C. W. Nielson, *Phys. Fluids* **13**, 2103 (1970).
- [57] R. Lichters, R. E. W. Pfund, and J. Meyer-ter-vehn, *A parallel one dimensional relativistic electromagnetic particle-in-cell code for simulating laser plasma interaction*, Max Planck Institute, Garching, Germany, <http://www.lichters.net/work.html>.
- [58] H. Ruhl, *Classical particle simulations*, in: *Introduction to Computational Methods in Many Body Physics*, M. Bonitz, D. Semkat (Eds.), (Rinton Press, 2006); K. Germaschewski, W. Fox, N. Ahmadi, L. Wang, S. Abbott, H. Ruhl, A. Bhattacharjee, *The Plasma Simulation Code: A modern particle-in-cell code with load-balancing and GPU support*, <http://arxiv.org/abs/1310.7866v1>.
- [59] A. Pukhov, *J. Plasma Phys.* **61**, 425-433 (1999).
- [60] K. J. Bowers, B. J. Albright, L. Yin, B. Bergen, T. J. T. Kwan, *Physics of Plasmas* **15**, 055703 (2008).
- [61] R. A. Fonseca, L. O. Silva, F. Tsung, V. K. Decyk, W. Lu, C. Ren, W. B. Mori, S. Deng, S. Lee, T. Katsouleas, et al., *OSIRIS: A three-dimensional, fully relativistic particle in cell code for modeling plasma based accelerators*, in: *(Computational Science-ICCS 2002, Springer, pp. 342 - 351)*.
- [62] C. Nieter, J. R. Cary, *Journal of Computational Physics* **196**, 448 (2004).
- [63] T. Umeda, Y. Omura, T. Tominaga, H. Matsumoto, *Computer Physics Communications* **156**, 73 (2003).
- [64] D. M. Sullivan, *Electromagnetic Simulation Using the FDTD Method*, 2nd Edition, (Wiley-IEEE Press, 2013).
- [65] V. L. Ginzburg, *Propagation of electromagnetic waves in plasma*, (Pergamon Press, Oxford, 1970).
- [66] B. A. Trubnikov, *Particle Interactions in a Fully Ionized Plasma*, in: *Reviews of Plasma Physics*, Vol. 1, M. A. Leontovich, Ed., (Consultants Bureau, New York, 1965).
- [67] G.J. Pert, *J Phys B* **38**, 27 (1999).
- [68] B. I. Cohen, A. M. Dimits, D. J. Strozzi, *Journal of Computational Physics* **234**, 33 (2013).
- [69] L. Spitzer Jr., *Physics of Fully Ionized Gases* (Interscience Publishers, New York, 1956).
- [70] C. D. Decker, W. B. Mori, J. M. Dawson, and T. Katsouleas, *Phys. Plasmas* **1**, 4043 (1994).